Asian Journal of Pharmaceutical Sciences 18 (2023) 100856

Available online at www.sciencedirect.com

ScienceDirect

journal homepage: www.elsevier.com/locate/AJPS

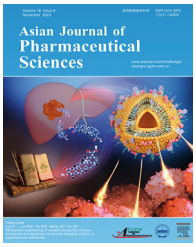

Original Research Paper

# Unleashing the healing potential: Exploring next-generation regenerative protein nanoscaffolds for burn wound recovery

*Liangwei Si*[a,1], *Xiong Guo*[a,1], *Hriday Bera*[a,b], *Yang Chen*[a], *Fangfang Xiu*[a], *Peixin Liu*[a], *Chunwei Zhao*[a], *Yasir Faraz Abbasi*[a], *Xing Tang*[c], *Vito Foderà*[d,*], *Dongmei Cun*[a,*], *Mingshi Yang*[a,d,*]

[a] *Wuya College of Innovation, Shenyang Pharmaceutical University, Shenyang 110016, China*
[b] *Dr. B. C. Roy College of Pharmacy and Allied Health Sciences, Durgapur 713206, India*
[c] *Department of Pharmaceutics, School of Pharmacy, Shenyang Pharmaceutical University, Shenyang 110016, China*
[d] *Department of Pharmacy, Faculty of Health and Medical Sciences, University of Copenhagen, Universitetsparken 2, DK-2100 Copenhagen O, Denmark*

ARTICLE INFO

*Article history:*
Received 18 June 2023
Revised 15 September 2023
Accepted 7 October 2023
Available online 21 October 2023

*Keywords:*
Regenerative proteins
α-lactalbumin
Serotonin
Electrospinning
Nanofibrous dressing
Third-degree burn

ABSTRACT

Burn injury is a serious public health problem and scientists are continuously aiming to develop promising biomimetic dressings for effective burn wound management. In this study, a greater efficacy in burn wound healing and the associated mechanisms of α-lactalbumin (ALA) based electrospun nanofibrous scaffolds (ENs) as compared to other regenerative protein scaffolds were established. Bovine serum albumin (BSA), collagen type I (COL), lysozyme (LZM) and ALA were separately blended with poly(ε-caprolactone) (PCL) to fabricate four different composite ENs (LZM/PCL, BSA/PCL, COL/PCL and ALA/PCL ENs). The hydrophilic composite scaffolds exhibited an enhanced wettability and variable mechanical properties. The ALA/PCL ENs demonstrated higher levels of fibroblast proliferation and adhesion than the other composite ENs. As compared to PCL ENs and other composite scaffolds, the ALA/PCL ENs also promoted a better maturity of the regenerative skin tissues and showed a comparable wound healing effect to Collagen sponge® on third-degree burn model. The enhanced wound healing activity of ALA/PCL ENs compared to other ENs could be attributed to their ability to promote serotonin production at wound sites. Collectively, this investigation demonstrated that ALA is a unique protein with a greater potential for burn wound healing as compared to other regenerative proteins when loaded in the nanofibrous scaffolds.



* Corresponding authors.
*E-mail addresses:* vito.fodera@sund.ku.dk (V. Foderà), cundongmei@163.com (D.M. Cun), mingshi.yang@sund.ku.dk (M.S. Yang).
[1] These authors contributed equally to this work.
Peer review under responsibility of Shenyang Pharmaceutical University.

https://doi.org/10.1016/j.ajps.2023.100856

## 1. Introduction

Severe burn commonly causes physically debilitating injuries, which could affect almost every organ in patients, leading to severe morbidity and mortality. Approximately 11 million people worldwide are severely burned each year and require extensive medical attention [1]. The burn injuries could be categorized according to their severity and depth of the skin injury. The superficial burns reach only up to the epidermal surfaces of the skin, causing redness. The partial-thickness burns result in the damage to the epidermis and part of the dermis layers of skin. Third-degree burn wounds are recognized as severe injuries, destroying almost all the skin layers, which are extremely challenging to manage [2]. Limited by sufficient skin autografts, severely burned patients often require appropriate wound dressings, which could contribute to adequate adhesion, migration, attachment and proliferation of fibroblast cells and promote angiogenesis, causing effective wound healing management [3]. A wide range of wound dressings including films, hydrogels, foams *etc.* are available in the market [4,5]. As compared to others, nanofibrous dressings are special scaffolds extensively employed for the management of severe burn wounds (*i.e.,* third-degree burns) owing to their unique properties such as high-surface area, nano-porosity, excellent air permeability and good barrier property for the protection of the wounds from infections and dehydration [6]. These nanofiber dressings could be accomplished through different techniques, such as self-assembly, electrospinning and thermal induced protocols [7]. Among these methods, the electrospinning technique is widely chosen due to its scalability, simplicity, cost-effectiveness and versatility. Electrospun nanofibrous scaffolds (ENs) resembled to the extracellular matrix (ECM) structure could provide a support for keratinocyte and fibroblast adhesion and help them to migrate to the wound sites, healing the damaged tissues [8].

Several biocompatible and biodegradable synthetic polymers, such as polycaprolactone (PCL), polylactic acid (PLA) and poly(D, L-lactide-co-glycolide) (PLGA), *etc.* have been employed to fabricate ENs [9]. Among these, PCL has recently been overexploited in fabricating nanofiber dressings due to its excellent spinnability and outstanding mechanical property. However, PCL ENs exhibited hydrophobic surface characteristics, limiting cells adherence and spreading. To overcome these hitches, the hydrophilic protein or other bio-polymer blended PCL based composite ENs are often fabricated [8]. In our continuous search of novel multifunctional biological materials with promising wound healing potentials, $\alpha$-lactalbumin (ALA) based nanofiber dressings as therapeutically active scaffolds promoting deep second-degree burn wound healing effects were recently developed and reported [2]. However, its specific mechanisms of action on deep burn wound healing activity still remain unclear. ALA is a 14.2 kDa whey protein existing in milk. It is a tryptophan-rich protein and acts as a precursor of neurotransmitter serotonin [10]. Several recent studies provided evidence that the serotonin could promote skin wound healing in burn patients by enhancing proliferation and migration of fibroblasts and promoting angiogenesis [11–13]. Enhanced serotonin production and neovascularization assisted burn wound healing activity of ALA as compared to other regenerative proteins such as lysozyme (LZM), bovin serum albumin (BSA), and collagen type I (COL) are urgently required to be verified.

LZM shares 40% amino acid sequence with ALA and has a closer spatial structure and gene organization to ALA [14]. This could eliminate bacteria and reduce inflammation when used in tissue regeneration. On the other hand, BSA is derived from cow blood and used as a nutrient in cell culture due to its biocompatibility, biodegradability, and non-toxicity. The biohybrid nanofiber dressings containing BSA could enhance physicochemical properties as well as bioactivity of the PCL based nanofibers to stimulate the wound healing process [15]. Furthermore, COL, a primary constituent of the skin ECM, has long been applied in skin tissue regeneration [16]. It is considered a gold standard graft material and widely employed in various marketed and clinically available skin dressings such as Alloderm®, Integra®, Matriderm® [17].

Although the biofunction of ALA in wound healing has been proved, it is necessary to explore whether the bioactivity of ALA in promoting burn wound healing is due to its unique properties or the common properties of protein materials. Therefore, in this research, four proteins (BSA, COL, LZM and ALA) were blended separately with PCL to fabricate different composite ENs and their distinguishing features compared to pure PCL ENs were examined through a series of *in vitro* characterizations. Their wound healing performances were further evaluated on fibroblasts and third-degree burn wound rat model. Moreover, the serotonin levels at wound sites and the ability of different ENs to promote tissue maturation on the animal model were investigated and compared to reveal the mechanisms of ALA based ENs behind their accelerated third-degree burn wound healing potentials.

## 2. Materials and methods

### 2.1. Materials

ALA (≥ 92.5%) was friendly provided by Davisco Food International, USA. LZM (20,000 U/mg), BSA (≥ 98%) and COL (> 90%) were purchased from MeilunBio (Dalian, China). PCL (Mn = 80,000, Sigma Aldrich, MO, USA), hexafluoroisopropanol (HFIP, Rhawn, Shanghai, China). FITC-phalloidin, DAPI and glutaraldehyde were purchased from Solarbio (Beijing, China). $\alpha$-MEM culture medium, DAPI and RIPA lysis buffer were purchased from Meilunbio. Anti-CD31 and anti-$\alpha$-SMA were obtained from Proteintech (IL, USA). Fetal bovine serum (FBS) was obtained from Gibco (NY, USA). Cy3-conjugated anti-rat IgG and FITC-conjugated anti-rat IgG were purchased from Servicebio (Wuhan, China). Collagen sponge® was obtained from BIOT Biology (Wuxi, China).

### 2.2. Fabrication of protein/PCL and pure PCL based ENs

Various composite ENs were accomplished based on our previous protocol [2]. Briefly, different proteins (BSA, COL, LZM and ALA) and PCL (1:3, w/w) were dissolved in HFIP and stirred overnight at room temperature to obtain transparent

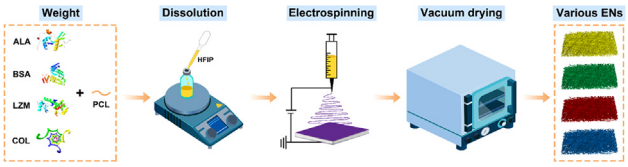


**Scheme 1 – Diagrammatic sketch of various composite ENs preparation procedures.**

spinning solutions. The resulting solutions were filled into 5.0 ml syringes and fixed on an electrospinning machine (Ucalery, Beijing, China), operating at a high electrical voltage of 15 kV with a feeding rate of 0.4 ml/h. The distance from the needle tip to the roller collector (100 r/min) was set to 15 cm. The electrospinning process was performed under controlled environmental conditions (25 ± 5 °C and 40% ± 10% RH). Following collecting the composite ENs, these were vacuum dried for 72 h to remove the residual solvent (Scheme 1). The pure PCL ENs were fabricated following a similar method but without blending proteins.

### 2.3. *Morphology and fiber diameter*

The morphology of the ENs was assessed by exploiting a field emission scanning electron microscopy (FESEM, ZEISS GEMINI 300, Germany). The ENs were sputter-coated with an Au-Pd layer and were then observed under a FESEM, functioning at a voltage of 12 kV. The average fiber diameter of ENs was determinized by analyzing the FESEM images of more than 100 different fibers by Image J software (National Institutes of Health, MD, USA).

### 2.4. *Physicochemical characterizations*

The diffraction patterns of ENs were recorded on powder X-ray diffraction (XRD, Rigaku ULTIMA IV, Japan) with Ni filtered Cu-K radiation, operating at voltage of 45 kV and input current of 40 mA. The samples were scanned within $2\theta$ range of 3° - 50° at the scanning rate of 1°/min. The thermograms of several scaffolds were recorded on a differential scanning calorimetry (DSC, TA DSC250, USA). Various samples (~5 mg) were hermetically sealed in an aluminum pan and scanned between 0 °C and 280 °C at a heating rate of 10 °C/min. The intermolecular interactions between protein and PCL in ENs were investigated by Fourier transform infrared spectroscopy (FTIR, Bruker, Germany) within wave number range of 4000–500 $cm^{-1}$.

### 2.5. *Proteins secondary structure analyses*

The changes of the secondary structures of different proteins (ALA, BSA, COL and LZM) during the electrospinning process were analyzed by Far UV circular dichroism (CD, Bio-Logic, France). The ENs (100 mg) were immersed in 5 ml PBS (pH 7.4) at 37 °C for 6 h to extract proteins. The protein content (ALA, BSA, COL and LZM) of various ENs was then determined by BCA protein assay kit (Beyotime, Shanghai, China). The CD spectra of different samples were obtained within 250–190 nm at a scanning speed of 50 nm/min [18]. The experimental CD data were further assessed using the BeStSel Web server to estimate secondary structural components of proteins, including $\alpha$-helix, $\beta$-sheet, and other contents [19].

### 2.6. *Wettability analysis*

The water contact angle (WCA) of the ENs was recorded using a contact angle goniometer (SINDIN, China). A drop of pure water (10 µl) was placed on the surfaces of the ENs, and the change of WCA over time was recorded.

### 2.7. *Water absorption rate*

The water absorption rate (WAR) of ENs was evaluated by a reported gravimetric method [20]. The ENs were cut into small pieces (1 cm × 1 cm), weighted ($W_{dry}$) and immersed in 8.0 ml PBS (pH 7.4) at 37 °C for 1 h. The samples were then carefully taken out of the medium and weighted ($W_{wet}$) after wiping off excess solution. The WAR was subsequently calculated according to Eq. 1:

$$\text{WAR}\ (\%) = \frac{W_{wet} - W_{dry}}{W_{dry}} \times 100\% \quad (1)$$

### 2.8. *Water vapor transmission rate*

The ASTM E96 method was adopted to determine the water vapor transmission rate (WVTR) of ENs [21]. The circular ENs (3.0 cm diameter) were fixed on the mouth of a glass bottle containing 4.5 ml pure water. The bottles were weighed and placed in a controlled chamber (CIMO, China) at 37 °C (relative humidity, 50%). Following 24-h incubation, the weights of these bottles were further recorded. The WVTR was then calculated using Eq. 2:

$$\text{WVTR}\left(g/m^2/d\right) = \frac{\Delta m}{\Delta t \times A} \quad (2)$$

Where $\Delta m$ represents the lost weight (g), $\Delta t$ denotes the time, and $A$ refers to the area of ENs exposed to the moisture transfer ($m^2$).

### 2.9. *Mechanical properties*

The thickness of the rectangular shaped ENs (10 mm × 20 mm) was measured using an electronic micrometer (Nscing Es, Nanjing, China). Their tensile properties (elongation, tensile strength and Young's modulus) were tested using a Texture Analyzer (Brookfield CT-3/4500, USA). These were attached with a load cell of 4,500 g, functioning at a strain rate of 0.2 mm/s at room temperature [2].

### 2.10. *Proliferation of fibroblasts*

The fibroblast (NIH-3T3) proliferation effects of various ENs were evaluated using Cell Counting Kit-8 (CCK-8, APExBIO, TX, USA) assay protocol [16]. Prior to the experiment, pure PCL ENs and different composite ENs were continuously soaked in 10 ml culture media for 7 d to extract their proteins.

Furthermore, the pure LZM, BSA, COL and ALA were dissolved in $\alpha$-MEM medium to prepare their solutions containing similar protein concentration (3.0 mg/ml) to that obtained after extraction of composite ENs. The fibroblasts were seeded in 96-well plates at a density of $2 \times 10^3$ cells/well and incubated in a $CO_2$ incubator for 24 h at 37 °C. The old media was discarded, replaced with different liquid extracts obtained from ENs and pure protein solutions and incubated for 24 h and 72 h. Subsequently, the cells were co-incubated with CCK-8 reagent (10 µl/well) for another 1.5 h and their optical density (OD) was recorded on a microplate reader (BMG LABTECH, Germany) at 450 nm. The cell viability was then calculated based on Eq. 3:

$$\text{Cell viability (\%)} = \frac{OD_{test}}{OD_{control}} \times 100\% \quad (3)$$

### 2.11. Adhesion of fibroblasts on ENs

Fibroblasts ($2.25 \times 10^4$ cells/well) were seeded onto ENs (diameter 20 mm) and fixed in a 12-well plate. After 48 h, the ENs containing adhered cells were collected and washed with PBS (pH 7.4) three times. The morphology of the adhered cells on ENs was then examined by laser scanning confocal microscope (LSCM) and FESEM [16]. For LSCM analyses, the ENs were incubated in 4% paraformaldehyde for 2 h and stained with FITC-phalloidin (100 nM) for 30 min. After washing with PBS, the ENs were further treated with nucleic stain, DAPI (10 µg/ml) for 10 min at room temperature. Subsequently, the images of the stained cells were captured on a confocal microscopy (Nikon Eclipse Ci H600L, Japan). On the other hand, for FESEM analysis, the ENs with attached cells were fixed with 2.5% glutaraldehyde for 2 h, washed three times with PBS and dried at ambient temperature for FESEM imaging.

### 2.12. Third-degree burn wound healing

Sprague-Dawley (SD) male rats (200 ± 10 g) were provided by the Experimental Animal Center of Shenyang Pharmaceutical University and used based on the Ethics Committee of Shenyang Pharmaceutical University. A third-degree burn wound rat model was developed following previous report with few modifications [22]. Precisely, 84 rats were anesthetized with chloral hydrate, and the metal punch (379.94 $mm^2$) of desktop super temperature control scalder (YLS-5Q, China) heated to 80 °C was tightly pressed on the shaved skin of the back of the rats at 10 kPa for 18 s to cause third-degree burn wounds. After 1 h, the full thickness dead skin was surgically removed using a scissor. Subsequently, a silicone ring was fixed around the wounds with special bio-glue (Gold elephant, China) to prevent wound contraction at the early stage. Various ENs were then placed onto the wounds using elastic bandages. The next day, the elastic bandages were removed and the ENs could tightly adhere onto the wounds without any physical support. The animals were then randomly divided into 7 groups ($n = 12$) and treated with blank control (without scaffolds), PCL ENs, LZM/PCL ENs, BSA/PCL ENs, COL/PCL ENs, ALA/PCL ENs and CS® (Collagen sponge®, positive control). Following treatment, the rats were housed alone at 25 °C. Gentamicin sulfate was added in the drinking water (0.15 g/l), and the cage cleanliness was strictly controlled during the study to prevent their bacterial infections. The rats were also weighed daily to monitor their wound infections [23]. The wound areas of control and different scaffolds treated groups were measured by capturing photographs at variable time points (7, 14 and 21 d) and the percentage of wound closure was calculated using Image J software. The simulation plots of wounds of treated animals were also obtained by exploiting Image J software [24]. Animals ($n \geq 3$) were sacrificed at 7, 14 and 21 d and their wound tissues were removed for further analyses.

### 2.13. Hematoxylin and eosin (H&E) staining

The skin samples collected after 7, 14 and 21 d treatment were fixed in 10% formalin solution, embedded in paraffin, and cut into 5 µm thick sections perpendicular to the wound surfaces. The representative sections of the skin were then stained with H&E for histological evaluation following the published protocol [25]. The length of the new epithelium of H&E stained tissues was measured to evaluate the effects of various ENs on epithelialization. The re-epithelialization rate (E%) was calculated according to Eq. 4:

$$E\ (\%) = \frac{L_i}{L_0} \times 100\% \quad (4)$$

Where, $L_0$ is the primitive wound length and $L_i$ refers to the length of new epithelium at the designated time point.

### 2.14. Serotonin content in the regenerate skin

Serotonin levels in the wound tissues of various ENs treated groups were estimated using ELISA kit (mlbio, Shanghai, China) according to the manufacturer's protocol [26]. Briefly, total protein in the wound tissues was isolated using RIPA lysis buffer containing protease inhibitor in an ice bath [22]. Then, samples (50 µl) and standard solutions (50 µl) were placed in the wells and the HRP-labeled antibody (100 µl) was subsequently introduced. The wells were then incubated for 60 min at 37 °C. Following washing, TMB substrate (50 µl) was added to the wells and incubated for 15 min at 37 °C. After adding the stop solution, the absorbance of the well contents was measured at 450 nm using a microplate reader.

### 2.15. Masson's trichrome staining

Following the previously described protocol, the tissue sections were stained with Masson's trichrome to assess the total collagen fibers at the wound sites. Images were captured with an optical microscope (Nikon Eclipse Ni-E, Japan) [22].

### 2.16. Sirius red staining

Sirius red staining was performed based on the reported procedure to distinguish types of collagen (collagen I and III) deposition in the samples [24]. Briefly, the tissue slices were stained with Biebrich scarlet dye for 10 min. These were

routinely dehydrated, transparentized using xylene, sealed using neutral gum, and observed under polarized microscope (Leica DM2700P, Germany). The quantitative ratio of collagen I/III was then analyzed by Image Pro-Plus 6.0 software (Media Cybernetics, MD, USA).

### 2.17. *Immunofluorescence staining*

Immunofluorescence staining was conducted to estimate angiogenesis at the healing wounds based on the previous protocol [24]. Paraffinic skin sections were incubated overnight with anti-CD31 (1:500) and anti-$\alpha$-SMA (1:300). The sections were then treated with Cy3-conjugated anti-rat IgG (1: 300) and FITC-conjugated anti-rat IgG (1: 300) for 50 min. Subsequently, these were stained with DAPI for 10 min and observed under a fluorescence microscope (Nikon Eclipse Ci H600L, Japan). The areas of blood vessels and mature blood vessels were calculated by Image J software.

### 2.18. *Statistical analyses*

All experimental data were presented as mean ± standard deviation (SD), and all experiments were repeated at least in triplicates. The data were analyzed by one-way ANOVA and Bonferroni's multiple comparison tests on the IBM SPSS statistics 17.0 software (International Business Machines Corp., NY, USA). A value of $P < 0.05$ was considered as statistically significant.

## 3. Results and discussion

### 3.1. *Fabrication and morphology of ENs*

In the current investigation, pure PCL ENs and various regenerative protein blended PCL based composite ENs (LZM/PCL, BSA/PCL, COL/PCL and ALA/PCL) as burn wound dressings were fabricated *via* electrospinning protocol. This technique utilized electrostatic force for affording nanofiber mats from homogeneous polymeric solutions [27]. At a constant liquid flow rate of 0.4 ml/h and electric field of 15 kV, a total solid content of 4.5% with protein/PCL mass ratio of 1:3 was observed most suitable for the electrospinning process as these were able to accomplish transparent and clear spinning solutions in HFIP (Fig. 1A). The plugging phenomenon was not observed during the electrospinning process for these solutions, which eventually produced nanofibrous mats with a smooth, uniform and flat appearance (Fig. 1A). There was no obvious difference in the appearance of each composite ENs, which was white and soft film. The representative FESEM images of all ENs depicted bead-free homogeneous nanofibers with smooth surfaces (Fig. 1B). The average diameter of nanofibers of pure PCL ENs was 307 ± 148 nm, while various composite ENs illustrated a drastically reduced fiber diameter. The diameter of the LZM/PCL ENs was larger, while other composite ENs were approximately 150 nm, with no significant difference. A smaller nanofiber diameter for the composite ENs might be due to the presence of various proteins (*i.e.*, zwitterionic molecules), which could enhance the stretching of ejected nanofibers due to their greater charge density. A variable diameter of nanofibers of different composite ENs could be attributed to their dissimilar levels of stretching during the electrospinning process [6].

### 3.2. *Physicochemical properties of ENs*

XRD patterns of pristine PCL ENs and various composite ENs were compared to examine their crystalline/amorphous states (Fig. 2A). The sharp diffraction peaks were absent in the XRD patterns of various pristine proteins, indicating their amorphous nature (Fig. S1) [28]. The XRD pattern of pure PCL scaffold showed a sharp and well-resolved XRD signal at 21.3° and a relatively low intensity peak at 23.7° [28]. This demonstrated that the crystalline characteristics of pure PCL was retained in its ENs (Fig. S1 and Fig. 2A) [29]. Various composite scaffolds also exhibited characteristic XRD signals of PCL with significantly attenuated intensity. This conferred the amorphization of PCL molecules in the composite ENs due to the incorporation of various proteins.

The DSC curves of various proteins did not exhibit obvious melting endotherms, implying their amorphous nature (Fig. S2). The DSC thermograms of native proteins displayed broad endothermic events at around 100 ºC ascribed to the water evaporation [30]. Pure PCL ENs illustrated an intense endothermic peak corresponding to the melting point of PCL appeared at 58 °C (Fig. 2B). A very shallow melting peak of PCL was evident in the composite ENs, which was a strong indication of the partial conversion of crystalline PCL molecules to their amorphous state in the presence of hydrophilic proteins [28]. The images obtained by polarizing light microscope also indicated that the PCL nanofibers had a certain level crystalline region [31]. When different proteins (LZM, BSA, COL, ALA) were added to the composite ENs, the crystallinity of PCL was significantly reduced (Fig. S3). These results were consistent with the XRD outcomes.

The FTIR spectrum of the pristine PCL showed a strong signal of carbonyl stretching vibration at 1725 $cm^{-1}$ (Fig. 2C). In addition, a prominent band near 1040 $cm^{-1}$ was ascribed to C–O–C stretching of PCL [32]. In the FT-IR spectra of native proteins, strong peaks within 3200–3400 $cm^{-1}$ were evidenced, which were attributed to their –OH stretching and the –NH stretching vibrations. Moreover, the bands about 1650 $cm^{-1}$ and 1520 $cm^{-1}$ represented their amide I and amide II vibration modes, respectively [32]. The FT-IR spectrums of various composite ENs illustrated characteristic peaks of PCL and proteins without any substantial shifting. These results implied that the proteins (LZM, BSA, COL, ALA) and PCL were successfully doped into the composite ENs and excluded the possibilities of the physical and chemical incompatibilities between proteins and PCL.

Raman spectroscopy was also used to characterize their intermolecular interactions. As shown in Fig. S4, the PCL ENs typical bands displayed at 1725 $cm^{-1}$ (C=O stretching), 1464 $cm^{-1}$ ($CH_2$ scissoring and wagging) and 1110 $cm^{-1}$ (C–O–C asymmetric stretching) [33]. Otherwise, the peaks near 1660 $cm^{-1}$ (Amide I), 1244 $cm^{-1}$ (Amide III) and 1006 $cm^{-1}$ (Phenylalanine peaks) could be attributed to various proteins (LZM, BSA, COL, ALA) [34]. No new peaks in different composite ENs, indicating that each protein was compatible with PCL.

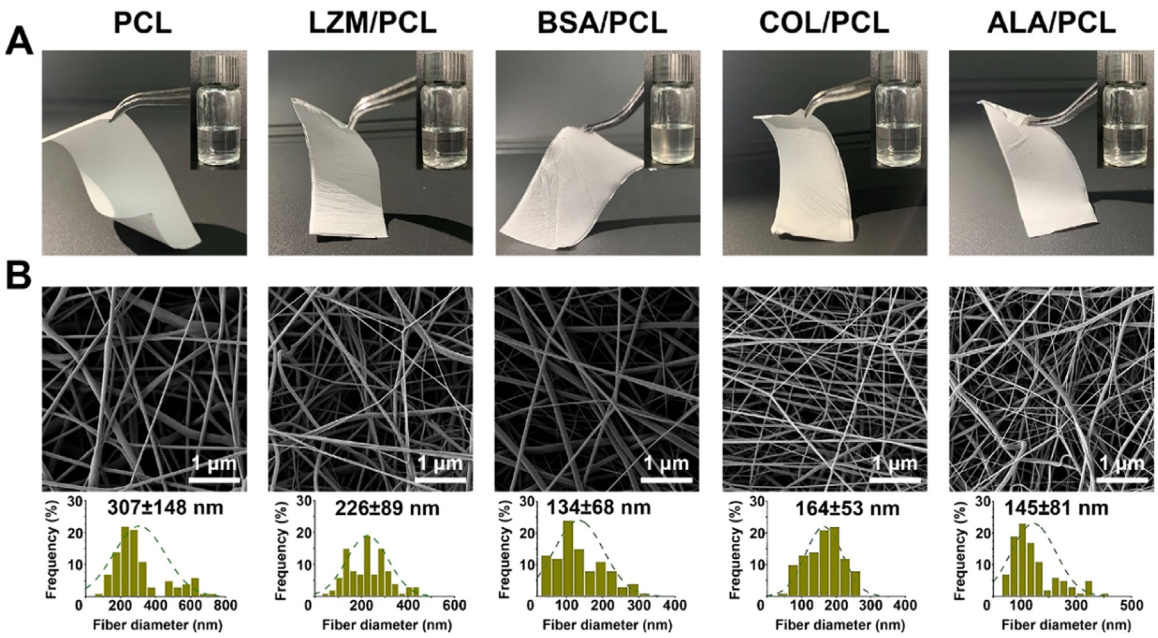


**Fig. 1 – (A) Appearance of various spinning solutions and their ENs. (B) FESEM images of different ENs illustrating their morphology and diameter distributions of the corresponding nanofibers.**

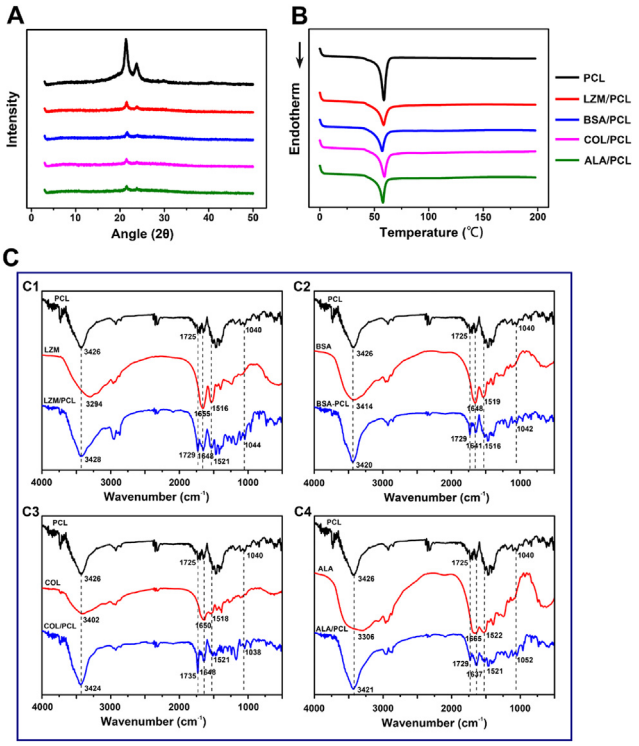


**Fig. 2 – (A) XRD patterns and (B) DSC curves of different ENs. (C) Overlay of FTIR spectra of composite ENs and their components (C1: PCL, LZM and LZM/PCL ENs; C2: PCL, BSA and BSA/PCL ENs; C3: PCL, COL and COL/PCL ENs, C4: PCL, ALA and ALA/PCL ENs).**

### 3.3. *Secondary structural configurations of proteins in ENs*

The results of the secondary structural configuration analyses of four different types of proteins isolated from ENs were assessed in PBS. The CD spectra of various proteins were further analyzed *via* the BeStSel Web server to estimate the contributions of specific secondary structural components in those samples [19]. As illustrated in Fig. 3A, the COL, LZM, BSA and ALA could retain their secondary structural configurations in the ENs, and the constitutive proportions of $\alpha$-helical and $\beta$-strand were not obviously changed as compared to their solution native forms [18,35,36]. Therefore, the electrospinning process had no apparent effects on the secondary structure of these proteins.

### 3.4. *Surface wettability of ENs*

WCA of various composite ENs over time was measured and compared with that of pure PCL ENs to assess the wettability of different hydrophilic proteins on the hybrid scaffolds (Fig. 3B). The composite ENs containing different hydrophilic proteins exhibited an improved wettability relative to that of PCL ENs. The WCA of the PCL ENs was not obviously changed within 120 s (from 106 ± 1° to 103 ± 1°). In contrast, composite scaffolds *viz.*, LZM/PCL, BSA/PCL, COL/PCL and ALA/PCL ENs demonstrated remarkably diminished WCA of 0°, 11° ± 2°, 50° ± 1° and 0°, respectively after 40 s. The hydrophilic proteins might have evenly amalgamated with hydrophobic PCL in the composite ENs, resulting in an enhancement of wettability of the hybrid nanofiber scaffolds [37]. An improved wettability of the composite ENs as compared to pristine PCL scaffolds might be beneficial for the adhesion, proliferation

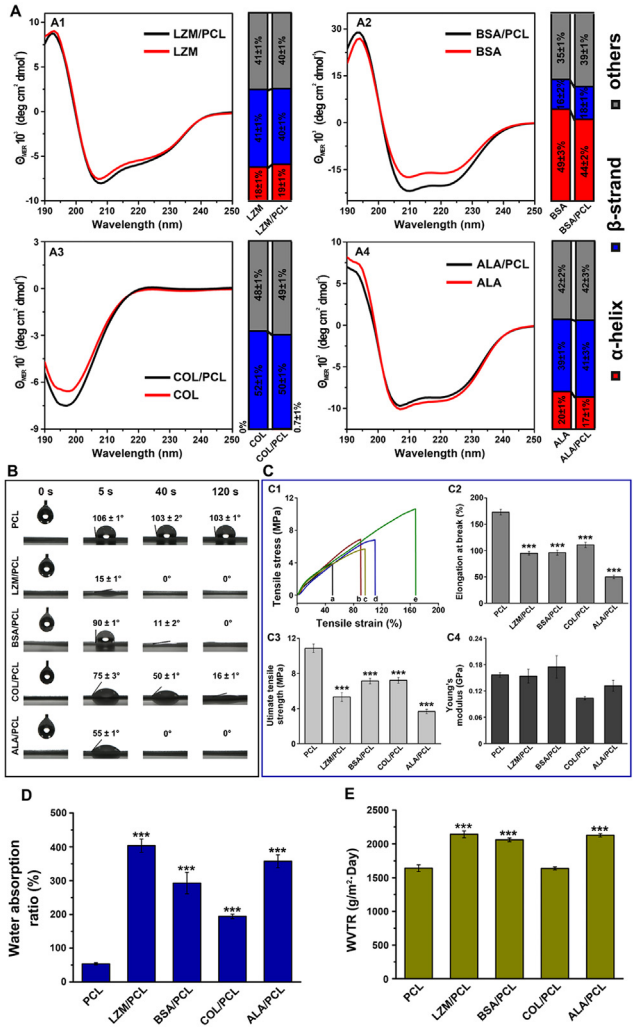


**Fig. 3 – (A) Far-UV CD spectra of proteins in PBS and various ENs (A1: LZM and LZM/PCL ENs; A2: BSA and BSA/PCL ENs; A3: COL and COL/PCL ENs; A4: ALA and ALA/PCL ENs) and corresponding secondary structural configuration data obtained from BeStSel. (B) WCA of different ENs at variable time points. (C) The mechanical properties of ENs including their (C1) strain-stress curves (a: ALA/PCL, b: BSA/PCL, c: LZM/PCL, d: COL/PCL, e: PCL), (C2) ultimate strain, (C3) ultimate tensile strength and (C4) Young's modulus. (D) Water absorption rate (WAR) and (E) water vapor transmission rate (WVTR) of different ENs. (*P < 0.05, **P < 0.01, ***P < 0.001, compared with PCL).**

and migration of fibroblasts during the wound healing process [38].

### 3.5. *Mechanical properties of ENs*

The mechanical strength of dressing is an essential parameter for the practical application which must be sufficient to prevent rupture during the dressing manufacturing process, as well as deformation, wear, and even damage caused by frequent joint movement and bending during use [39]. The composite ENs displayed extremely different mechanical properties as compared to pure PCL based ENs (Fig. 3C). Pristine PCL scaffolds were soft and flexible in nature with elongation, strength, Young's modulus of 172.76% ± 5.28%, 10.87 ± 0.49 MPa, and 0.16 ± 0.0052 GPa, respectively. On the other hand, composite ENs containing different proteins displayed a significantly decreased elongation and tensile strength ($P < 0.001$) with similar Young's modulus values relative to PCL ENs. The variable mechanical properties of composite ENs could be accredited to the different levels of interactions between PCL and proteins in the hybrid scaffolds [2,40]. Interestingly, the mechanical strength of pure PCL ENs and composite ENs would be appropriate enough to prevent tearing and other damages during handling and storage and could be applied to deep burn wound surfaces [41].

### 3.6. *Water absorption and water vapor transmission*

Generally, an ideal artificial skin scaffold could not only prevent the accumulation of excess wound exudates, but also control the rate of water evaporation to avoid excessive dehydration of the wounds [42]. Therefore, WAR and WVTR of all these ENs were assessed. As shown in Fig. 3D, the WAR values of hydrophilic protein blended composite ENs were significantly increased as compared to that of pristine PCL ENs ($P < 0.05$). Pure PCL based ENs had the lowest WAR of 53.71% ± 3.28%, while LZM/PCL ENs displayed the highest WAR of 403.4% ± 19.63%. Particularly, ALA/PCL ENs showed an adequate WAR value (357.4% ± 19.23%), which might be appropriate for controlling the moisture balance at the wound surfaces [42].

The optimal WVTR value of wound dressings should be within 2,000 - 2,500 g/m$^2$/d. A high WVTR value could result in wound dehydration, whereas a low WVTR value could cause exudate accumulation and increase the risk of bacterial infections [21]. Fig. 3E showed a clear trend of improving WVTR value for protein blended composite ENs (1,637 ± 22.24 - 2,142 ± 50.60 g/m$^2$/d) relative to the pure PCL ENs (1,641 ± 50.65 g/m$^2$/d). Possibly, the highly porous and network structures of the hydrophilic protein blended composite ENs could improve their WVTR values [43]. Furthermore, even after long exposure (*i.e.*, 14 d) in the aqueous environment the microscopic structures of all these ENs were well maintained with a slight interfacial adhesion among the fibers (Fig. S5). This signified that the ENs could sustain their structural integrity in the moist environment of the wounds for an extended period of time.

### 3.7. *Fibroblast proliferation and adhesion on ENs*

The results of the cell viability assay of liquid extracts of the ENs on murine NIH-3T3 cells exhibited their excellent tolerability on mammalian fibroblasts (Fig. 4A). All the ENs (LZM/PCL, BSA/PCL, COL/PCL and ALA/PCL) depicted negligible effects on cell growth as compared to the control group following 24 h of incubation. Interestingly, the BSA/PCL ENs and ALA/PCL ENs revealed significantly enhanced fibroblast proliferation after 72-h incubation ($P < 0.05$). The fibroblast proliferation effects of pure protein solutions containing the same protein contents (3.0 mg/ml) to that of ENs were

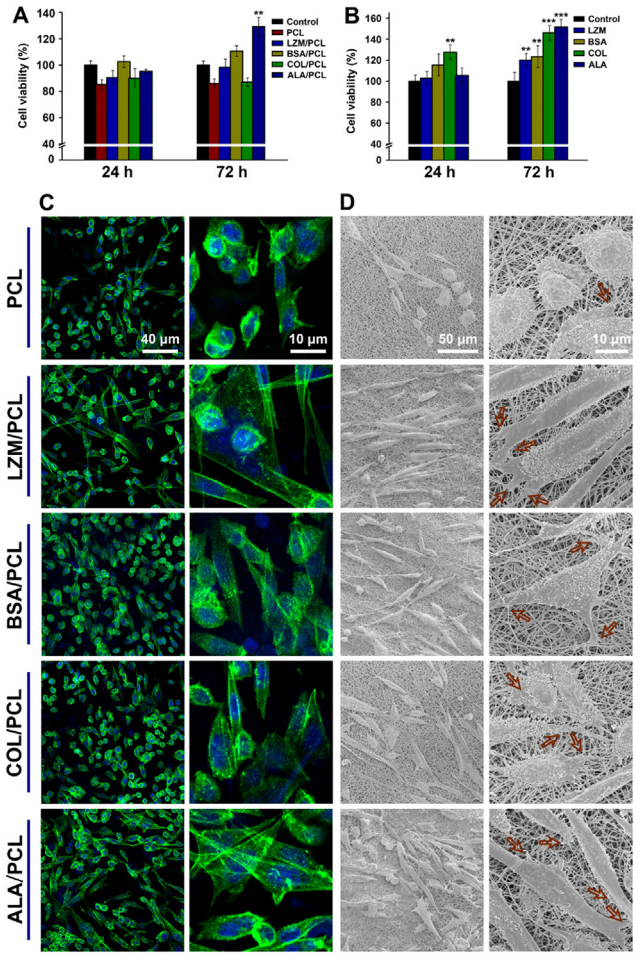


**Fig. 4 – (A) NIH-3T3 cell viability after treatment with liquid extracts of PCL ENs, and composite ENs (protein content, 3.0 mg/ml) following 24 h and 72 h of incubation (*P < 0.05, **P < 0.01, ***P < 0.001, compared with PCL). (B) The NIH-3T3 cell viability of pure protein solutions (protein content, 3.0 mg/ml) following 24 and 72 h of treatments (*P < 0.05, **P < 0.01, ***P < 0.001, compared with Control). (C) LSCM images of fibroblast adhesion and their morphology following 48 h of treatment with different ENs. (D) FESEM images of fibroblast adhesion and their morphology after 48 h of treatment with various ENs captured at different magnifications.**

further evaluated and illustrated in Fig. 4B. As compared to control group, different native proteins conferred a dramatically improved fibroblast proliferation after longer time of incubation and among different proteins, ALA showed the highest cell proliferation potential with average viability of 151% ± 5% after 72 h of incubation. These could be due to the fact that the enzymatic ALA degradation products could promote the proliferation of fibroblasts. The cell proliferation potentials of ALA hydrolysate and collagenase I and IV degraded ALA products on fibroblasts provided supportive evidences to our hypothesis (Fig. S6).

The fibroblast adhesion properties on the fabricated scaffolds were investigated by LSCM studies (Fig. 4C). The cells showed a well-spread morphology onto the composite ENs as compared to the control PCL ENs. Significantly higher hydrophilic surfaces of the composite scaffolds could favor the cells adhesion relative to the pure PCL ENs [32]. Among various composite scaffolds, the ALA/PCL ENs displayed the greatest distribution density of the fibroblast cells proliferated along the fibers. These outcomes were consistent with the FESEM results (Fig. 4D), portraying an improved adhesion and spreading morphology of the fibroblast cells onto the composite ENs. The fibroblasts were clustered and produced pseudopodia onto the composite scaffolds, displaying better cell adhesion [16]. In addition, the bio-mimicking nature and nano-topography of the composite ENs represent a natural environment for improving cell adhesion [44]. The cells acquired a better morphological spindle shape in case of ALA/PCL ENs as compared to other composite ENs and pure PCL ENs [45].

### 3.8. *In vivo deep burn wound healing*

Based on our earlier study, the third-degree burn wound rat model was successfully established [2]. In this context, a burning time of 18 s was found appropriate according to the H&E staining images of the wounds. Some parts of the dermis layer were still retained for shorter burning time (12 s). On the other hand, when the burning time was increased over 20 s, the muscle layers of animals were partially destroyed (Fig. S7). The animals bearing third-degree burn wounds were randomized into several groups and treated with fabricated ENs. Their *in vivo* wound healing effects were studied exploiting various experimental protocols (Fig. 5A). The animals without receiving any treatment were considered as blank control group. In contrast, the rats treated with CS®, a collagen sponge dressing which is one of the few commercially available protein-based wound dressings, was chosen as positive control group. All the scaffolds were cut into circles with diameter of 22.0 mm and applied onto the burn wounds. Before applying various scaffolds, the silicone rings with inner diameter of the splint of 31.0 mm were fixed around the burn wounds to prevent rodent skin contraction (Fig. 5B).

Fig. 5C and 5D displayed the timely changes in the macroscopic appearances of the wounds during their healing process. After 21-d treatment, the color of the wound skin of ALA/PCL ENs treated group was significantly improved as compared to that of other scaffold treated groups. The wound closure rates of various groups of animals were recorded as a function of time (Fig. 5C). The wound closure rates of different scaffold treated groups became smaller than the control group after 14 d, while their wound size remained almost similar to that of control group after 7 d. Various scaffolds treated animals displayed obviously improved wound closure rate compared to the control group ($P < 0.05$) after 21 d treatment. Interestingly, the animals bearing ALA/PCL ENs exhibited the fastest wound closure rate with the smallest wound area relative to the other ENs and positive CS® groups. ALA/PCL ENs could be used as a favorable dressing for burn wound healing due to the stable nanofibrous structure provided by PCL polymer and the excellent bioactivity of ALA. There was no significant difference in the body weights among all the animal groups during this experiment (Fig. 5F), indicating

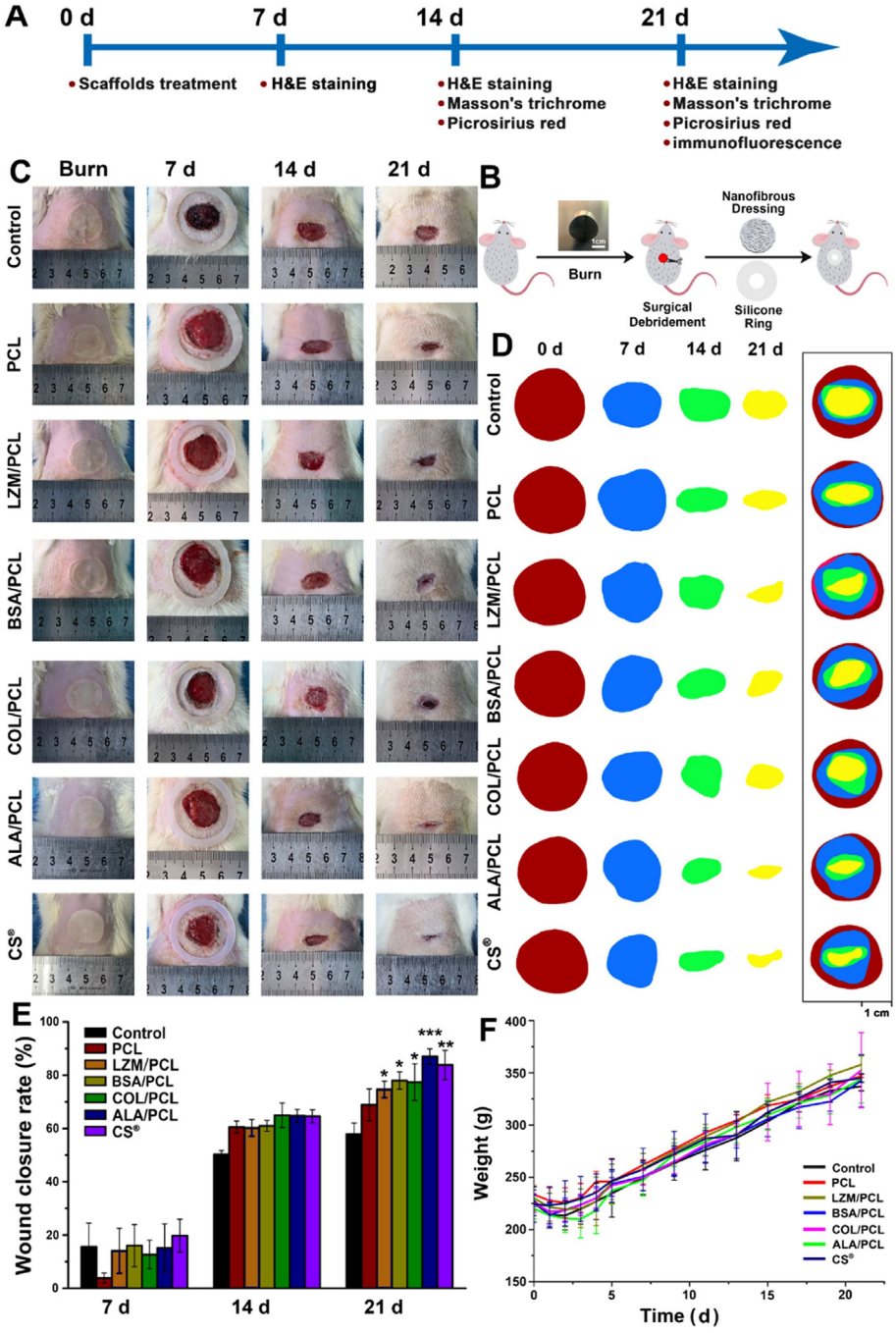


**Fig. 5 – (A) Schematic representation of various experimental protocols for evaluating the wound healing potentials of ENs on third-degree burn rat models. (B) Critical steps involved in developing third-degree burns rat models and the application of ENs on the burn wounds. (C) Representative appearances and (D) simulation plots of wounds of various animal groups treated with blank control, different ENs and commercial dressing: CS® over time. (E) Wound closure rates of various groups (*$P < 0.05$, **$P < 0.01$, ***$P < 0.001$, compared with PCL). (F) The body weight changes of each group during the wound healing process.**

the healthy conditions of the rats during the wound healing process [46].

### 3.9. *H&E staining*

To assess the wound healing efficacy of different dressings, the H&E staining images of the sectioned tissues at variable time points were analyzed further and their results were compared in Fig. 6A. After 7-d treatment, the granulation tissues of all the groups were in intense local inflammatory state owing to the infiltration of neutrophils and macrophages (Open square mark) [47]. The inflammation was still noticed even after 14d of treatment, but the epidermis layers of various groups started crawling (black solid line). However,

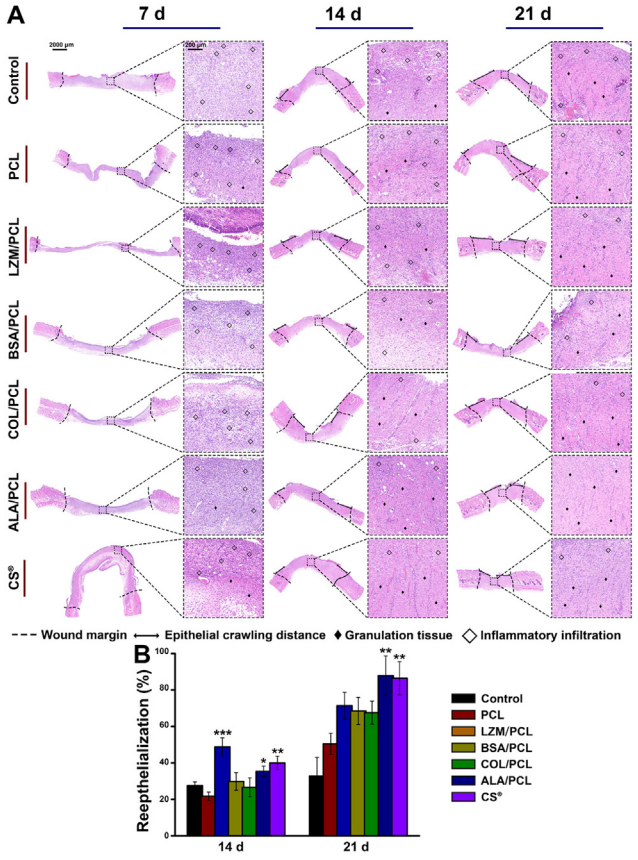


**Fig. 6 – (A) H&E staining images of various groups treated with ENs, illustrating their wound healing capacities with time. (B) Quantitative histological analyses of re-epithelization of different groups after 14 and 21 d of treatments (*P < 0.05, **P < 0.01, ***P < 0.001, compared with PCL).**

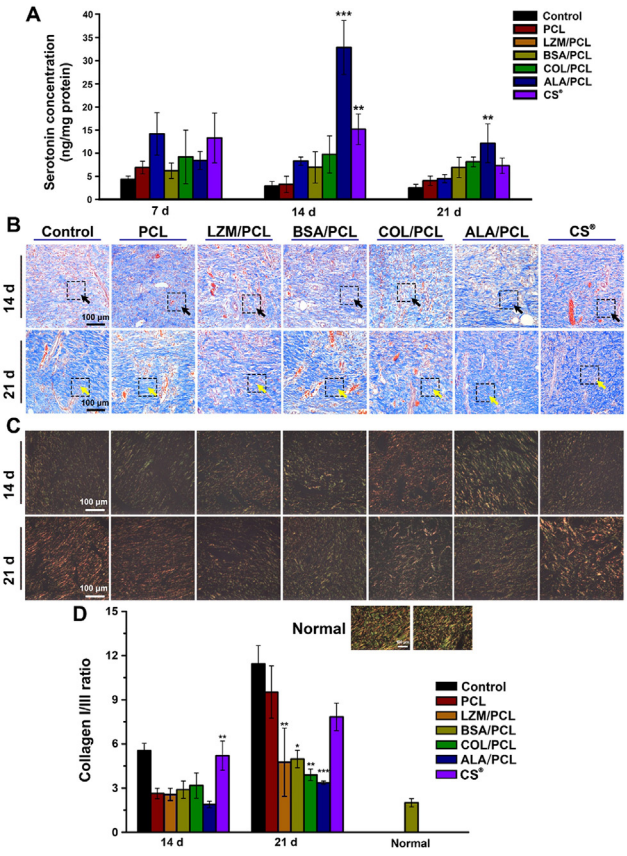


**Fig. 7 – (A) Changes of serotonin contents in the regenerative skin tissues of different groups after 7, 14 and 21 d of treatments (*P < 0.05, **P < 0.01, ***P < 0.001, compared with PCL). (B) Representative images of tissues after Masson trichrome staining, exhibiting collagen deposition after 14 and 21 d of treatments (black arrows showed immature collagen and yellow arrows indicated mature collagen). (C) Representative images of collagen fibers stained with PSR after 14 and 21 d of treatments. (D) Quantitative analysis of the collagen I/III ratios of various groups treated with ENs and CS® (*P < 0.05, **P < 0.01, ***P < 0.001, compared with PCL).**

the ALA/PCL ENs treated group displayed an attenuated level of inflammation, which could be attributed to the special apoptosis promoting effects of ALA on the senescent cells [48]. Prominently, the wounds treated with the ALA/PCL ENs were almost closed after 21 d of treatment and eventually their abilities to promote neotissue regeneration and maturation were better than the other groups. Following treatment with various ENs, the epithelial cell growth rates of their corresponding groups were quantified (Fig. 6B). Notably, the ALA/PCL ENs treated group showed a similar epidermal crawling rate (88.0% ± 10.8%) to that of the CS® treated group (86.5% ± 9.1%) after 21-d treatment, while it was significantly higher as compared to other composite ENs (LZM/PCL ENs: 71.4% ± 7.3%, BSA/PCL ENs: 68.5% ± 6.6%, COL/PCL ENs: 67.6% ± 6.3%) ($P < 0.05$). Plausibly, ALA could suppress nociception and inflammation *in vivo*, accelerating wound healing rate [49].

### 3.10. *Mechanisms of ENs in burn wound healing*

#### 3.10.1. *Serotonin production at wound sites*

The mechanisms of improved burn wound healing capacity of ALA/PCL ENs were further explored as compared to other regenerative proteins. It has been reported that ALA is rich in tryptophan, which is the precursor of neurotransmitter serotonin synthesis [10]. A higher level of serotonin causes the proliferation of fibroblasts, deposition of collagen and neovascularization, resulting in an improved burn wound healing effect [12,13]. To validate the wound healing mechanisms of ALA/PCL ENs, the serotonin contents in the wound tissues following treatment with various scaffolds were initially estimated (Fig. 7A). There were no significant differences in serotonin levels among all the treatment groups at the early stages of wound healing process. After 14-d treatment, the serotonin content at the wound sites of ALA/PCL ENs treated group was significantly higher than that in other groups ($P < 0.05$). It implied that ALA could potentially promote serotonin production, which could play a crucial role in the wound healing process [11,50]. Even after 21 d, the serotonin levels in the ALA/PCL ENs

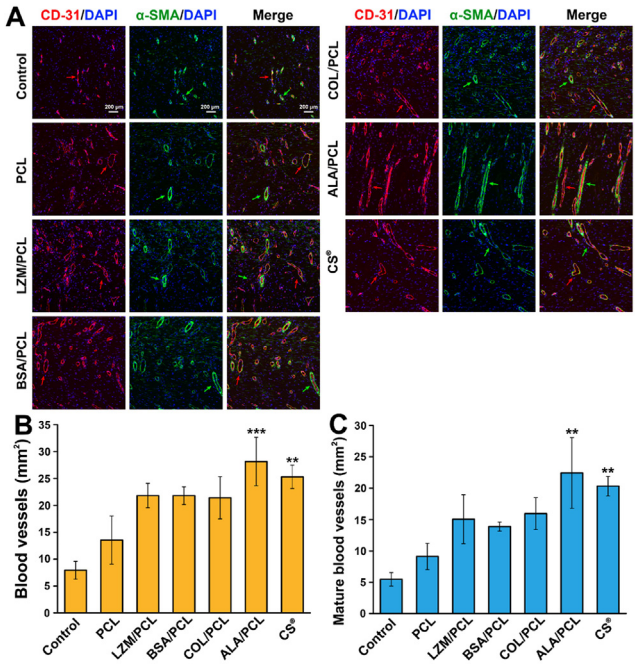


**Fig. 8 – (A) The images of wound tissues after dual immunofluorescence staining (α-SMA and CD31), portraying extent of angiogenesis in various groups treated with ENs and CS®. Morphometric analyses of (B) new blood vessels and (C) mature blood vessels at the wound sites following treatment (*P < 0.05, **P < 0.01, ***P < 0.001, compared with PCL).**

treated group remained remarkably greater than that in other composite ENs and positive control groups. As ALA/PCL ENs could facilitate the synthesis of serotonin at the wound sites, these could accelerate the burn wound healing rate with improved maturity of the wound tissues [11,26].

### 3.10.2. *Collagen deposition*

In order to evaluate the efficacy of different ENs on wound healing, the deposition of total collagen and its types (collagen I and III) at the wound sites were further investigated using Masson trichrome staining and Picrosirius Red (PSR) staining, respectively. The collagen fibers appeared in blue, while the muscle fibers were spotted in red in the images of Masson's trichrome staining (Fig. 7B). The ALA/PCL ENs and CS® treated groups portrayed an enhanced collagen deposition than that of control and other composite scaffolds treated groups after 14-d treatment. The collagen in ALA/PCL ENs treated group became more mature than those in others with increasing healing time (Fig. 7B). The scar thicker collagens (black arrows) were arranged parallel to the skin surfaces, while the dense mature collagens (yellow arrows) were often deposited in a basket weave pattern [51].

In the birefringence images of wound tissues, type I collagen emerged in yellow or red, whereas the thicker type III collagen appeared in green (Fig. 7C) and the ratios of collagen I and III were further quantified for each treated group (Fig. 7D) [24]. The collagen I/III ratios in each group were augmented after 14-d treatment, which might be due to the increased production of type I collagen [51]. As the wounds matured after 21 d, the collagen I/III ratio of ALA/PCL ENs treated group was significantly lower than that of other groups ($P < 0.05$) and closer to that observed in normal tissues. Thus, it clearly evidenced that the ALA/PCL ENs could remarkably improve the maturity of the skin regenerative tissues [2].

### 3.10.3. *Promotion of angiogenesis*

The extent of wound tissue angiogenesis of each group was investigated by dual immunofluorescence staining of CD31 and α-SMA after 21-d treatment (Fig. 8A). Angiogenesis is an important process during wound healing, which could assist in replacing damaged capillaries and consequently, restore the supply of adequate oxygen and nutrients to the wound tissues. CD31 is a vital marker of the endothelial cells in the blood vessels, while α-SMA is expressed in the smooth muscle layers of the blood vessels. The immunofluorescence staining illustrated that the density and number of blood vessels (red arrows) in the ALA/PCL ENs treated group and positive control group were significantly higher than those in the pure PCL ENs and other composite ENs treated groups ($P < 0.05$) (Fig. 8B). Moreover, the ALA/PCL ENs treated group showed a better vascular maturity than the other scaffold treated groups ($P < 0.01$) (Fig. 8C). The maturation of the vascular network with larger vessels would be crucial for the wound tissue micro-environments in their remolding stages [52]. An enhanced neovascularization potential of ALA/PCL ENs could be accredited to their ability of serotonin production at the wound sites [13].

## 4. Conclusions

In this study, different proteins (COL, BSA, LZM and ALA) were blended with PCL to afford composite ENs *via* electrospinning process. The therapeutic effects of various ENs at the cellular level and on third-degree burn wound rat model were systematically investigated. ALA/PCL ENs depicted favorable physico-chemical characteristics and improved therapeutic benefits in burn wound management as compared to other composite ENs (COL/PCL, BSA/PCL, LZM/PCL) and pure PCL ENs. ALA/PCL ENs could assist collagen maturation, improve collagen I/III ratios and vascular maturity by increasing the serotonin production in the wound tissues. The stable nanofibrous structure contributed by PCL and the excellent bioactivity of ALA rendered that ALA /PCL ENs could be used as an encouraging dressing for burn wound healing. In summary, ALA was a special protein and has a better therapeutic prospect than other regenerative proteins (LZM, BSA and COL) when applied in the third degree burn wound healing management. In the future, it will be necessary to investigate how ALA molecules work at the burn wound site, whether as ALA molecules or as its hydrolyzed or enzymatic fragments.

## Conflicts of interest

The authors report no conflicts of interest. The authors alone are responsible for the content and writing of this article.

## Acknowledgements

This work was financially supported by the Liaoning Pan Deng Xue Zhe Scholar (No. XLYC2002061) and the Overseas Expertise Introduction Project for Discipline Innovation ("111 Project") (No. D20029). X. G. acknowledges the Educational Department of Liaoning Province (grant No. LJKZ0925), (Youth Project, grant No. LJKQZ2021035), and the international postdoctoral exchange fellowship program (grant No. PC2021047). H. B. thanks the financial support from National Natural Science Foundation of China (grant No. 82050410448) and Fellowship of China Postdoctoral Science Foundation (grant No. 2021MD703857). D.Cun acknowledges financial support from Ministry of Education Chunhui Program (2020). VF acknowledges VILLUM FONDEN for supporting the project via the Villum Young Investigator Grant (grant No. 19175).

## Supplementary materials

Supplementary material associated with this article can be found, in the online version, at doi:10.1016/j.ajps.2023.100856.

## References

[1] Jeschke MG, van Baar ME, Choudhry MA, Chung KK, Gibran NS, Logsetty S. Burn injury. Nat Rev Dis Primers 2020;6(1):25.
[2] Guo X, Liu YN, Bera H, Zhang HT, Chen Y, Cun DM, et al. Alpha-lactalbumin-based nanofiber dressings improve burn wound healing and reduce scarring. Acs Appl Mater Interfaces 2020;12:45702–13.
[3] Wu H, Zhang R, Hu BX, He YT, Zhang YH, Cai L, et al. A porous hydrogel scaffold mimicking the extracellular matrix with swim bladder derived collagen for renal tissue regeneration. Chin Chem Lett 2021;32:3940–7.
[4] Norahan MH, Pedroza-Gonz SC, Sanchez-Salazar MG, Alvarez MM, Stantiago GTD. Structural and biological engineering of 3D hydrogels for wound healing. Bioact Mater 2023;24:197–235.
[5] Sun A, He XY, Ji X, Hu DR, Pan M, Zhang LH, et al. Current research progress of photopolymerized hydrogels in tissue engineering. Chin Chem Lett 2021;32:2117–26.
[6] Shi S, Si YF, Han YT, Wu T, Iqbal MI, Fei B, et al. Recent progress in protective membranes fabricated via electrospinning: advanced materials, biomimetic structures, and functional applications. Adv Mater 2022;34.
[7] Loo HL, Goh BH, Lee LH Chuah LH. Application of chitosan-based nanoparticles in skin wound healing. Asian J Pharm Sci 2022;17(3) 299-32.
[8] Krysiak ZJ, Stachewicz U. Electrospun fibers as carriers for topical drug delivery and release in skin bandages and patches for atopic dermatitis treatment. Wires Nanomed Nanobi 2023;15(1):35.
[9] Liang YQ, Liang YP, Zhang HL, Guo BL. Antibacterial biomaterials for skin wound dressing. Asian J Pharm Sci 2022;17(3):353–84.
[10] Layman DK, Lonnerdal B, Fernstrom JD. Applications for alpha-lactalbumin in human nutrition. Nutr Rev 2018;76:444–60.
[11] Sadiq A, Shah A, Jeschke M, Belo C, Qasim Hayat M, Murad S, et al. The role of serotonin during skin healing in post-thermal injury. Int J Mol Sci 2018;19.
[12] Mann DA, Oakley F. Serotonin paracrine signaling in tissue fibrosis. Biochimica Et Biophysica Acta-Molecular Basis of Disease 2013;1832:905–10.
[13] Sadiq A, Menchetti I, Shah A, Jeschke MG, Belo C, Carlos-Alcalde W, et al. 5-HT1A receptor function makes wound healing a happier process. Front Pharmacol 2018;9.
[14] Zhang TT, Zhou PH, Zhan YF, Shi XW, Lin JY, Du YM, et al. Pectin/lysozyme bilayers layer-by-layer deposited cellulose nanofibrous mats for antibacterial application. Carbohydr Polym 2015;117:687–93.
[15] Homaeigohar S, Monavari M, Koenen B, Boccaccini AR. Biomimetic biohybrid nanofibers containing bovine serum albumin as a bioactive moiety for wound dressing. Mater Sci Eng C 2021:123.
[16] Qian YZ, Zhou XF, Zhang FM, Diekwisch TGH, Luan XH, Yang JX. Triple PLGA/PCL scaffold modification including silver impregnation, collagen coating, and electrospinning significantly improve biocompatibility, antimicrobial, and osteogenic properties for orofacial tissue regeneration. Acs Appl Mater Interfaces 2019;11:37381–96.
[17] Ho J, Walsh C, Yue D, Dardik A, Cheema U. Current advancements and strategies in tissue engineering for wound healing: a comprehensive review. Adv Wound Care 2017;6:191–209.
[18] Stie MB, Corezzi M, Bombin ADJ, Ajalloueian F, Attrill E, Pagliara S, et al. Waterborne electrospinning of alpha-lactalbumin generates tunable and biocompatible nanofibers for drug delivery. Acs Appl Nano Mater 2020;3:1910–21.
[19] Micsonai A, Wien F, Bulyaki E, Kun J, Moussong E, Lee YH, et al. BeStSel: a web server for accurate protein secondary structure prediction and fold recognition from the circular dichroism spectra. Nucleic Acids Res 2018;46:W315–WW22.
[20] Shi R, Geng H, Gong M, Ye JJ, Wu CG, Hu XH, et al. Long-acting and broad-spectrum antimicrobial electrospun poly (epsilon-caprolactone)/gelatin micro/nanofibers for wound dressing. J Colloid Interface Sci 2018;509:275–84.
[21] dos Santos DM, Leite IS, Bukzem AD, Santos RPD, Frollini E, Inada NM, et al. Nanostructured electrospun nonwovens of poly(epsilon-caprolactone)/quaternized chitosan for potential biomedical applications. Carbohydr Polym 2018;186:110–21.
[22] Yergoz F, Hastar N, Cimenci CE, Ozkan AD, Tekinay T, Guler MO, et al. Heparin mimetic peptide nanofiber gel promotes regeneration of full thickness burn injury. Biomaterials 2017;134:117–27.
[23] Olfert ED, Godson DL. Humane endpoints for infectious disease animal models. ILAR journal 2000;41:99–104.
[24] Shen YF, Xu GZ, Huang HX, Wang KY, Wang H, Lang MD, et al. Sequential release of small extracellular vesicles from bilayered thiolated alginate/polyethylene glycol diacrylate hydrogels for scarless wound healing. ACS Nano 2021;15:6352–68.
[25] Tang Q, Lim T, Wei XJ, Wang QY, Xu JC, Shen LY, et al. A free-standing multilayer film as a novel delivery carrier of platelet lysates for potential wound-dressing applications. Biomaterials 2020:255.
[26] Slominski AT, Kim TK, Kleszczynski K, Semak I, Janjetovic Z, Sweatman T, et al. Characterization of serotonin and N-acetylserotonin systems in the human epidermis and skin cells. J Pineal Res 2020:68.
[27] Xue JJ, Wu T, Dai YQ, Xia YN. Electrospinning and electrospun nanofibers: methods, materials, and applications. Chem Rev 2019;119:5298–415.
[28] He M, Jiang HY, Wang R, Xie Y, Zhao CS. Fabrication of metrpnidazole loaded poly (epsilon-caprolactone)/zein core/shell nanofiber membranes via coaxial electrospinning for guided tissue regeneration. J Colloid Interface Sci 2017;490:270–8.

[29] Gautam S, Dinda AK, Mishra NC. Fabrication and characterization of PCL/gelatin composite nanofibrous scaffold for tissue engineering applications by electrospinning method. Mater Sci Eng C 2013;33:1228–35.
[30] Chen ZG, Wang PW, Wei B, Mo XM, Cui FZ. Electrospun collagen-chitosan nanofiber: a biomimetic extracellular matrix for endothelial cell and smooth muscle cell. Acta Biomater 2010;6:372–82.
[31] Zhu KJ, Li Y, Jiang HL, Yasuda H, Ichimaru A, Yamamoto K, et al. Preparation, characterization and *in vitro* release properties of ibuprofen-loaded microspheres based on polylactide, poly(epsilon-caprolactone) and their copolymers. J Microencapsul 2005;22:25–36.
[32] Ahmed SM, Ahmed H, Tian C, Tu Q, Guo YD, Wang JY. Whey protein concentrate doped electrospun poly(epsilon-caprolactone) fibers for antibiotic release improvement. Colloids Surf B Biointerfaces 2016;143:371–81.
[33] Gao X, Zhang XH, Song JL, Xu X, Xu AX, Wang MK, et al. Osteoinductive peptide-functionalized nanofibers with highly ordered structure as biomimetic scaffolds for bone tissue engineering. Int J Nanomed 2015;10:7109–28.
[34] Tarhan O, Tarhan E, Harsa S. Investigation of the structure of alpha- lactalbumin protein nanotubes using optical spectroscopy. J Dairy Res 2014;81:98–106.
[35] Jiang HL, Hu YQ, Li Y, Zhao PC, Zhu KJ, Chen WL. A facile technique to prepare biodegradable coaxial electrospun nanofibers for controlled release of bioactive agents. J Control Release 2005;108:237–43.
[36] Zhang Q, Lv S, Lu JF, Jiang ST, Lin L. Characterization of polycaprolactone/collagen fibrous scaffolds by electrospinning and their bioactivity. Int J Biol Macromol 2015;76:94–101.
[37] Steffi C, Wang D, Kong CH, Wang ZY, Lim PN, Shi ZL, et al. Estradiol-loaded poly(epsilon-caprolactone)/silk fibroin electrospun microfibers decrease osteoclast activity and retain osteoblast function. Acs Appl Mater Interfaces 2018;10:9988–98.
[38] Ma K, Chan CK, Liao S, Hwang WYK, Feng Q, Ramakrishna S. Electrospun nanofiber scaffolds for rapid and rich capture of bone marrow-derived hematopoietic stem cells. Biomaterials 2008;29:2096–103.
[39] Monfared-Hajishirkiaee R, Ehtesabi H, Rezaei A, Najafinobar S. Development of carboxymethyl cellulose/chitosan double-layer hydrogel combining myrtle essential oil and thyme honey to enhance antibacterial and mechanical properties. J Ind Eng Chem 2023;126:382–97.
[40] Aguirre-Chagala YE, Altuzar V, Len-Sarabia E, Tinoco-Magaa JC, Yaez-Limn JM, Mendoza-Barrera C. Physicochemical properties of polycaprolactone/collagen/elastin nanofibers fabricated by electrospinning. Mater Sci Eng C 2017;76:897–907.
[41] Jin GR, Prabhakaran MP, Kai D, Annamalai SK, Arunachalam KD, Ramakrishna S. Tissue engineered plant extracts as nanofibrous wound dressing. Biomaterials 2013;34:724–34.
[42] Rezaei A, Ehtesabi H. Fabrication of alginate/chitosan nanocomposite sponges using green synthesized carbon dots as potential wound dressing. Mater Today Chem 2022;24:12.
[43] Aydogdu A, Sumnu G, Sahin S. A novel electrospun hydroxypropyl methylcellulose/polyethylene oxide blend nanofibers: morphology and physicochemical properties. Carbohydr Polym 2018;181:234–46.
[44] Brennan DA, Conte AA, Kanski G, Turkula S, Hu X, Kleiner MT, et al. Mechanical considerations for electrospun nanofibers in tendon and ligament repair. Adv Healthc Mater 2018;7.
[45] Puhl DL, Mohanraj D, Nelson DW, Gilbert RJ. Designing electrospun fiber platforms for efficient delivery of genetic material and genome editing tools. Adv Drug Del Rev 2022;183:114161.
[46] Xu SB, Chang LN, Hu YA, Zhao XJ, Huang SC, Chen ZH, et al. Tea polyphenol modified, photothermal responsive and ROS generative black phosphorus quantum dots as nanoplatforms for promoting MRSA infected wounds healing in diabetic rats. J Nanobiotechnology 2021;19.
[47] Saleh B, Dhaliwal HK, Portillo-Lara R, Shirzaei Sani E, Abdi R, Amiji MM, et al. Local immunomodulation using an adhesive hydrogel loaded with miRNA-laden nanoparticles promotes wound healing. Small 2019:15.
[48] Kohler C, Hakansson A, Svanborg C, Orrenius S, Zhivotovsky B. Protease activation in apoptosis induced by MAL. Exp Cell Res 1999;249:260–8.
[49] Yamaguchi M, Yoshida K, Uchida M. Novel functions of bovine milk-derived alpha-lactalbumin: anti-nociceptive and anti-inflammatory activity caused by inhibiting cyclooxygenase-2 and phospholipase A(2). Biol Pharm Bull 2009;32:366–71.
[50] de las Casas-Engel M, Corbi AL. Serotonin modulation of macrophage polarization: inflammation and beyond. Camps, J Ed; Adv Experiment Med Biol 2014;824:89–115.
[51] Pratsinis H, Mavrogonatou E, Kletsas D. Scarless wound healing: from development to senescence. Adv Drug Del Rev 2019;146:325–43.
[52] Algarrahi K, Franck D, Ghezzi CE, Cristofaro V, Yang XH, Sullivan MP, et al. Acellular bi-layer silk fibroin scaffolds support functional tissue regeneration in a rat model of onlay esophagoplasty. Biomaterials 2015;53:149–59.